# High-force magnetic tweezers with force feedback for biological applications

Philip Kollmannsberger and Ben Fabry
*Zentrum für Medizinische Physik und Technik, Universität Erlangen-Nürnberg, Henkestrasse 91, 91052 Erlangen, Germany*

(Received 10 August 2007; accepted 10 October 2007; published online 9 November 2007)

Magnetic micromanipulation using magnetic tweezers is a versatile biophysical technique and has been used for single-molecule unfolding, rheology measurements, and studies of force-regulated processes in living cells. This article describes an inexpensive magnetic tweezer setup for the application of precisely controlled forces up to 100 nN onto 5 $\mu$m magnetic beads. High precision of the force is achieved by a parametric force calibration method together with a real-time control of the magnetic tweezer position and current. High forces are achieved by bead-magnet distances of only a few micrometers. Applying such high forces can be used to characterize the local viscoelasticity of soft materials in the nonlinear regime, or to study force-regulated processes and mechanochemical signal transduction in living cells. The setup can be easily adapted to any inverted microscope. © *2007 American Institute of Physics.* [DOI: 10.1063/1.2804771]

## INTRODUCTION

Micromanipulation and microrheology techniques such as atomic force microscopy, micropipettes, microneedles, as well as optical and magnetic traps have important applications in biophysics and cell biology. The use of magnetic forces in biology dates back to the early 20th century, when Heilbronn, a botanist, inserted magnetic particles into protoplasts and observed their movement in a magnetic gradient.[1] Similar work was carried out by Freundlich and Seifriz in echinoderm eggs around the same time.[2] In 1949, Crick and Hughes characterized the viscoelastic response of chick fibroblasts,[3] and later Yagi[4] and Hiramoto[5] further refined the magnetic particle method as a tool to study the viscoelasticity of living cells. Since then, many researchers have utilized and improved different variants of the magnetic particle method as a tool for manipulating biomolecules, protein force spectroscopy, and microrheology studies in soft materials and cells.

Multidimensional magnetic tweezers with several magnetic poles that can be used to move magnetic particles in arbitrary directions[6–8] are the most versatile; however, they are limited by the magnitude of force that can be applied. The most flexible design so far has been the exchangable-pole magnetic trap recently developed by Fisher *et al.*,[9] in which the pole geometry can be changed depending on the requirements of the experiment.

Two-pole setups can be used to generate high and alternating forces between two opposing magnets.[10–13] Guilford and Gore[11] used optical tracking and current feedback in their two-pole magnetic trap and were able to apply forces of up to 80 nN on spherical metal particles of $>10$ $\mu$m diameter, suitable for tissue studies but not for single cell experiments.

Vertical magnetic tweezers use the vertical gradient between two magnetic poles placed above the sample stage. This geometry has been used for DNA unfolding experiments and adhesion studies, but, while generating homogenous gradient fields, it is limited in the range of applicable forces ($<0.2$ nN).[14–17] The highest forces are usually obtained with one-pole microneedle geometries, either implemented using permanent magnets[18] or electromagnets with soft iron cores.[19–22] Another fundamentally different type, not discussed here further, uses homogenous magnetic fields to rotate permanently magnetized particles (magnetic twisting).[23–25]

The aim of the present work was to increase the magnitude of applicable forces compared to earlier implementations of the magnetic tweezers method in an inexpensive and easily reproducible setup. It consists of a single solenoid with a high-permeability soft iron core attached to a remote-controlled micromanipulator. High forces of up to 100 nN onto 5 $\mu$m magnetic beads are achieved by distances between core and bead as small as 10 $\mu$m. An inherent problem of this design is the poor control of force due to the highly nonlinear force-distance relationship. We solved this problem by constantly tracking the distance between bead and core, and adapting the solenoid current and/or the core position using the micromanipulator. Force is calibrated using the classic viscous drag approach,[4] and an empirical fit is used to describe the nonlinear relationship between distance, current, and force with an analytical formula. This setup provides high timing and force accuracy, and can be adapted to all common inverted microscopes equipped with a charge coupled device (CCD) camera.

## SYSTEM DESIGN

An overview of the setup is shown in Fig. 1. The magnetic microneedle consists of a cylindrical rod made of high-permeability nickel alloy. If a magnetic bead with volume $V$

 

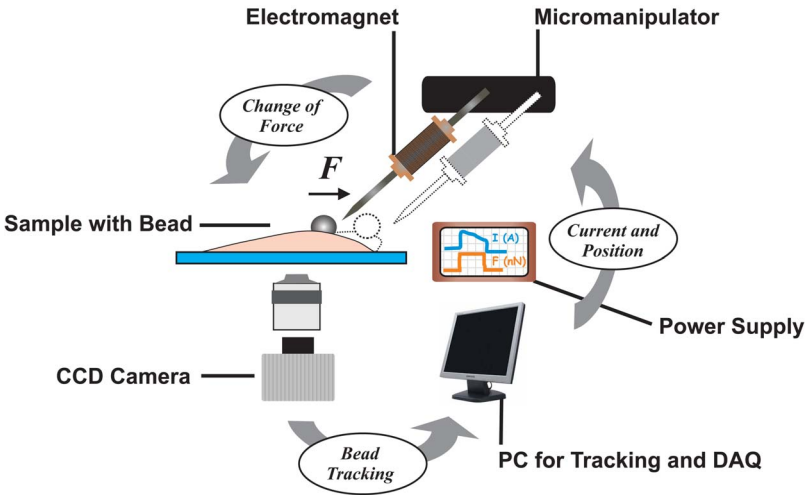


FIG. 1. (Color online) Schematic view of the setup. The $\mu$-metal core of a solenoid is attached to a micromanipulator on a microscope equipped with a heated $x$-$y$ stage, antivibration table, motorized $z$ drive and shutter, and a CCD camera connected to a PC. Solenoid current and core tip position are controlled by the PC, and bead positions are tracked in real time.

and magnetic susceptibility $\chi$ is exposed to an external magnetic field $\mathbf{H}=\mathbf{B}/\mu$, the field induces in the bead a magnetic moment

$$\mathbf{m}=\chi\times V\times\mathbf{H}. \tag{1}$$

If the magnetic field is inhomogenous ($\nabla\mathbf{B}\neq 0$), the probe experiences a gradient force,

$$\mathbf{F}=\left(\mathbf{m}\cdot\frac{\partial}{\partial\mathbf{r}}\right)\mathbf{B}. \tag{2}$$

The limiting factors for $F$ are the magnetic moment of the probe, which is determined by its size and susceptibility as well as the magnitude of the applied magnetic field, and the gradient of the field. The field magnitude can be increased by increasing the solenoid current or number of coil turns until the core is saturated. The permeability $\mu(H)$ of the core is a material parameter which determines the total magnetic flux through the core at a certain external field. Thus, the core material should be selected for the highest possible permeability, as well as lowest hysteresivity. The gradient strength depends on the geometry of the core. If the core is needle shaped, the magnetic flux is bundled and the gradient will reach a maximum near the needle tip.

Data shown here were obtained with a core material of either HyMU-80 (Carpenter Technology, Reading, PA) or Mumetall (Vacuumschmelze GmbH, Hanau, Germany). The core has a diameter of 4.5 mm and a length of 100 mm. One end is tapered and has a sharp tip with radius of $<10$ $\mu$m. Tapering is done using a diamond grinder, and the tip is polished using #4000 grade sandpaper. The magnetic field is generated by a solenoid, which consists of 200 turns of 0.5 mm copper wire on a brass frame enclosing the microneedle, and is connected to a power supply. The microneedle is attached to an Eppendorf InjectMan NI-2 micromanipulator (Eppendorf AG, Hamburg, Germany) for precise positioning with an accuracy of 40 nm. The micromanipulator has a RS-232 interface and can be remote controlled by a personal computer (PC). The magnetic flux density of the microneedle is monitored by a miniature Hall probe (SS496A, Honeywell, Morristown, NJ) attached to the rear end of the core.

The current source for the solenoid current is custom built and can generate a current of up to 3 A at an output power of 35 W. It consists of an OPA-549 high current operational amplifier (Texas Instruments, Dallas, TX) powered by a regulated power supply in a voltage-to-current conversion circuit.

Bright-field images of bead and needle tip are taken by a CCD camera (Orca-ER, Hamamatsu GmbH, Herrsching) at frame rates of 40 Hz. For simultaneous imaging of the structure of living cells or other specimens that are probed, illumination can be switched to dark field or epifluorescence during experiments either manually or using remote-controlled shutters and filter wheels. In these modes, however, bead positions cannot be tracked real time.

The voltage signal for controlling solenoid current and the image acquisition trigger signal are generated by a PC equipped with a 16 bit data acquisition board (NI-6052E, National Instruments, Austin, TX). For every captured frame, solenoid current and magnetic flux density are simultaneously recorded using the analog-to-digital (AD) converter of the NI-6052E board. The CCD camera is triggered using the card's timer output. Image acquisition and driving current are synchronized, and a hardware generated transistor-transistor logic (TTL) pulse is used to define the start of an experiment.

Software for image acquisition, bead tracking and control of the electromagnet was programmed in C++ as a standalone application under WINDOWS XP using the VISUAL.NET development environment and can be obtained from the authors upon request. Drivers for CDD camera and the AD/DA board were supplied by the manufacturer. Even though the program used here was developed for the Hamamatsu digital camera application programming interface (DCAM) protocol, the National Instruments data acquisition (DAQ) boards, the Eppendorf InjectMan micromanipulator, and for Leica microscopes, the software can be easily adapted to other hardware or operating system platforms and does not depend on any specific software environment or host application.

Positions of one or more beads in the field of view are determined by pattern matching and then tracked through subsequent frames using an intensity-weighted center-of-mass algorithm.[26] The position of the needle tip in the field

TABLE I. Comparison of different types of beads in terms of force-to-volume ratio. Force is given for a driving current of 3 A and a bead-to-needle distance of 20 $\mu$m.

| | Bangs Labs (Compel beads) | Spherotech (CFM-40-10) | Invitrogen (Dynabeads M-450) | Custom $Fe_3O_4$ (ferrimagnetic) |
|---|---|---|---|---|
| Diameter | 5.8±0.2 $\mu$m | 4.9±0.3 $\mu$m | 4.5±0.2 $\mu$m | 4.5±0.2 $\mu$m |
| $F$ at 3 A, 20$\mu$m | 2 nN | 3.5 nN | 12 nN | 60 nN |
| $F/V$ | 0.02±0.002 nN/$\mu$m$^3$ | 0.08±0.01 nN/$\mu$m$^3$ | 0.25±0.03 nN/$\mu$m$^3$ | 1.25±0.17 nN/$\mu$m$^3$ |

of view is determined by erosion and dilation operations on a downscaled image, followed by thresholding and segmentation, yielding a binary image of needle and background that is then used to find the needle position. Bead and needle positions, the current, and the magnetic flux density for every image taken are written to a text file. Images are acquired into a frame buffer in the PC memory at 40 frames per second and can optionally be stored on hard disk for later analysis.

## FORCE FEEDBACK

Driving current or needle position can be changed after every frame in order to react to changes in bead position (Fig. 1). This ensures accurate force control even for bead-needle distances of only a few micrometers. Without force feedback, the bead movement towards the magnet would lead to a steeply increasing force and, possibly, to contact between the bead and the magnet. For distances of more than 20 $\mu$m, the nonlinearity of the force-distance relationship is less pronounced, and it is sufficient to update the driving current only. For shorter distances, however, it is necessary to move the needle as well. The reaction time of the control mechanism is limited by the camera frame rate (up to 40 Hz) for current updates, and by the response time of the micromanipulator to RS232 commands (~50 ms) for the needle position.

## CALIBRATION AND VALIDATION

### Force calibration

Force is calibrated by measuring the velocity of a bead moving through a viscous fluid, as described elsewhere.[4] A small number of the beads to be calibrated are diluted in uncured PDMS with known viscosity $\eta$ between 0.1 and 10 Pa s (factory-calibrated poly(dimethylsiloxane), Sigma-Aldrich, St. Louis, MO). The needle is then immersed into the solution, and bead movements are tracked during repeated current on-off cycles, each on or off phase lasting 1 s. Settling of the viscous fluid causes a bead drift, which we determine during the current-off phases. The force acting on a bead during the current-on phase was then computed from the drift-corrected velocities $\mathbf{v}$ according to Stokes' formula for viscous drag,

$$\mathbf{F} = 6\pi \times \eta \times r \times \mathbf{v}. \quad (3)$$

The radius $r$ of the beads used here (Table I) had standard deviations of less than 0.2 $\mu$m between beads as determined with optical and scanning electron microscopy. Force-distance curves for multiple beads and currents are recorded, and a simple mathematical expression is fitted to the data of all beads, distances, forces, and currents (Fig. 2),

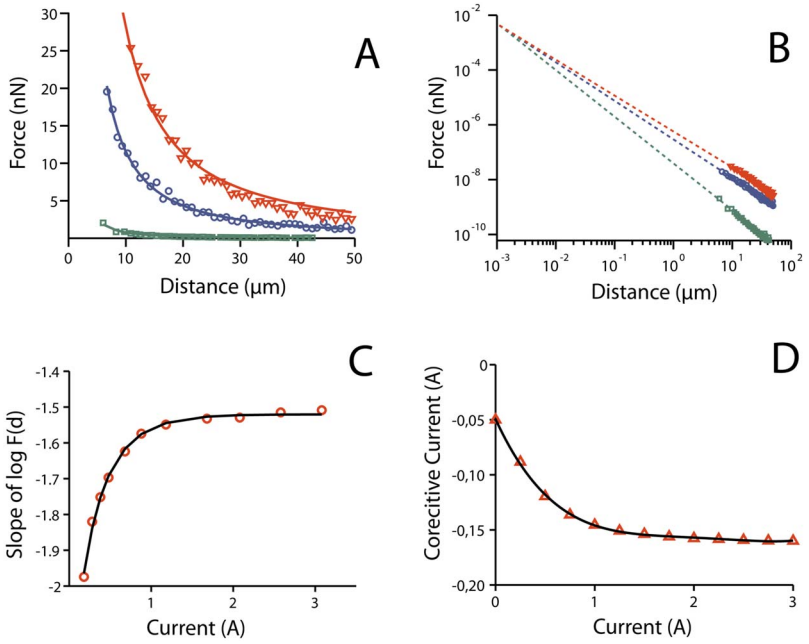


FIG. 2. (Color online) (A) force-distance curves are recorded at different currents (shown here: 100, 600, and 2500 mA) for 4.5 $\mu$m superparamagnetic beads (Invitrogen Dynabeads). (B) Fitting Eq. (4) to all data points yields a common intersection of the force-distance curves from multiple currents. Note that in a double-logarithmic plot, the force-distance curves form straight lines. (C) Equation (5) is fitted to the slopes of the double-logarithmically plotted force-distance curves (i.e., the power-law exponent of the force-distance relationship) at different currents. At high currents, both beads and pole tip are saturated and the slope flattens out. (D) coercitive currents for different magnetization currents are recorded and fitted by a fourth-order polynomial to compensate for the magnetic hysteresis of the solenoid core material.

$$F(d,I) = F_0 \times \left(\frac{d}{d_0}\right)^{c(I)}. \quad (4)$$

Equation (4) describes the relationship between force $F$, current $I$, and distance $d$, using two scaling parameters ($F_0$ and $d_0$) for force and distance, and a current-dependent distance exponent, $c(I)$, describing the slope of the $F$-$d$ curve in a log-log plot. For instance, $c=-2$ corresponds to $F \sim 1/d^2$ and $c=-1$ to $F \sim 1/d$. This current-dependent exponent is fitted to the function

$$c(I) = \frac{c_1}{1 + c_2 \times \exp(c_3 \times I)}, \quad (5)$$

using three parameters $c_{1\ldots3}$. With a total of five parameters, this calibration formula accurately describes the force at any measured distance and current. Equation (4) can be rearranged to compute the driving current that is necessary to obtain a desired force at any given distance between the bead and the needle,

$$I(F,d) = 1/c_3 \times \ln\left\{1/c_2 \times \left(c_1 \times \left[\frac{\ln(d/d_0)}{\ln(F/F_0)}\right] - 1\right)\right\}. \quad (6a)$$

Alternatively, Eq. (4) can be rearranged to compute the needle position (i.e., the bead-needle distance) that is necessary to obtain a desired force at a given current,

$$d(F,I) = d_0 \times \left(\frac{F}{F_0}\right)^{1/b(I)}. \quad (6b)$$

Equations (6a) and (6b) are at the core of the force feedback mechanism described above.

### Angle dependence

The magnitude of the magnetic field gradient, and hence the force magnitude, depends crucially on the shape of the needle tip. Highest forces and steepest gradients are obtained using the smallest possible tip radius. The direction of forces was found to point always to the surface normal of the tip. That means that, for beads within an angle of about 120° around the tip and a distance not higher than 100 $\mu$m from the tip, the force vector points towards the center of the circle describing the tip (Fig. 3). For these beads, the magnitude of force depends only on the Euclidean distance to the tip, and is independent of the bead position relative to the needle axis. This feature of the force-distance relationship greatly simplifies the force calibration procedure and magnetic tweezer experiments. For instance, without loss of accuracy, the forcing direction and the needle axis need not be precisely aligned, and the needle tip can be moved a few micrometer above the $z$ plane of the bead to avoid contact between the needle and the substrate to which the bead adheres.

### Characterization of beads

Until some years ago, the large variations of magnetic susceptibility in commercialy available magnetic beads made accurate force calibration impossible.[11] Nowadays, this no longer seems to be an issue. We compared superparamagnetic and ferrimagnetic beads from different suppliers. Best results in terms of force-to-volume ratio were obtained for superparamagnetic 4.5 $\mu$m Invitrogen Dynabeads and 4 $\mu$m custom-made ferrimagnetic beads (Table I).

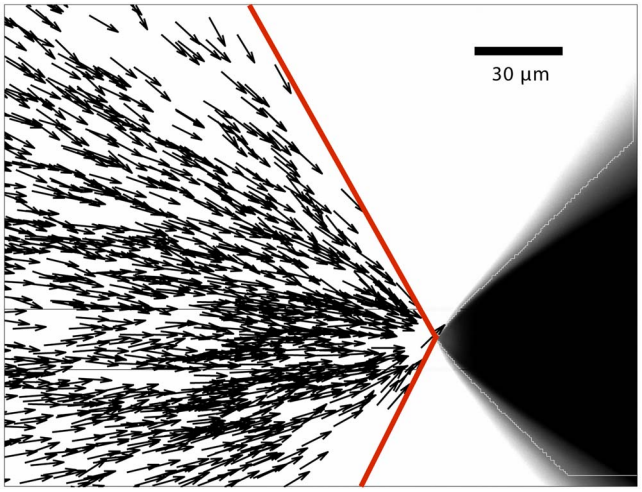


FIG. 3. (Color online) Force vectors point towards the needle tip. Force magnitude only depends on the bead-tip distance for all beads within a cone of about 120° around the tip (solid lines).

### Hysteresis compensation

Despite being superparamagnetic, the magnetic needle still shows some hysteresis, which means the magnetic flux does not completely vanish after switching off the current. The hysteresis can worsen if the needle heats up as a result of machining, such as lathing or grinding. One way to overcome this is by reannealing the needle material at high temperatures (>800 °C) which restores the superparamagnetic properties. Another way described here is to cancel the remanent magnetic field by superimposing a small compensation magnetic field generated by the solenoid. The magnitude of the coercitive current depends on the magnetic history of the material, i.e., the highest magnetic field strength it has been subjected to. We calibrated the compensation current that was necessary for hysteresis compensation in the following way. A Hall probe to monitor the magnetic flux through the core is attached to the proximal (blunt) end of the needle. After application of a brief (1 s) magnetization current pulse, the compensation current necessary to generate zero flux is determined. The relationship between magnetization current and compensation current is fit to a fourth-order polynomial in order to determine the necessary compensation current for any level of magnetization (Fig. 2). Between experiments, the magnetization of the core is erased by applying a sinusoidal voltage with decaying amplitude (de-Gaussing), which creates a random orientation of the permanent magnetic domains in the material and, hence, zero total flux.

### Timing

Driving current and camera shutter are precisely synchronized by a hardware clock signal. To ensure accurate timing and a fast onset of force despite the high inductivity of the coil, we monitored the actual coil current by measur-

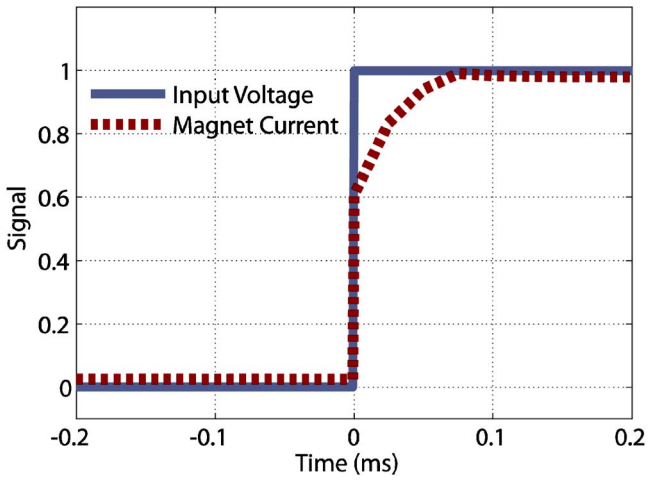


FIG. 4. (Color online) Solenoid current, and hence force, is delayed by less than 100 $\mu$s compared to the control voltage generated by the DA converter (DAC) board. This ensures that force application and image acquisition can be synchronized.

ing the voltage across a 1 Ω resistor in series to the solenoid. The rise time of the current and hence force was less than 100 $\mu$s (Fig. 4).

## DISCUSSION AND APPLICATIONS

### Open chamber design

The necessarily short distance between bead and magnet makes this design incompatible with a closed chamber design for live cell imaging, which limits the duration of experiments involving living cells or other specimens where contact to air has to be avoided. This limitation can be somewhat eased by using an open chamber and covering the surface with mineral oil after immersing the magnet, essentially sealing it from air contact while maintaining full maneuverability of the magnet. Another option is flushing the media with a constant stream of an air/$CO_2$ mixture.

### Force accuracy

The major source of error for force calculation is the distance between bead and magnet during calibration or tracking. For the calculation of the applied force using Eq. (4), an uncertainty $\Delta d$ in measuring the distance leads to a relative error in force reconstruction,

$$\frac{\Delta F}{F} = \sqrt{\left(\frac{\partial F(d,I)}{\partial d} \times \frac{\Delta d}{d}\right)^2} = \left| c(I) \times \frac{\Delta d}{d} \right|. \tag{7}$$

For a distance $d=10$ $\mu$m and an error $\Delta d=1$ $\mu$m, the relative error is between 15% and 20%, and becomes smaller for larger distances. The distance error and variations in bead diameter add up to a total relative error between 18% and 28% depending on bead type. This estimate agrees with the rms difference between our force-distance data points of beads (Fig. 2) and the predictions from Eq. (4).

## APPLICATIONS

A typical use of magnetic tweezers is the characterization of local viscoelastic properties of soft materials (microrheology). High forces are needed to study the nonlinear regime of viscoelasticity, where biological materials are known to exhibit various phenomena such as stiffening or yielding. We measured the bead displacement during application of a stepwise increasing force of up to 10 nN to beads attached to or embedded in a linear elastic medium (polyacrylamide gel) or a living cell [Figs. 5(a) and 5(b)]. For beads embedded in the polyacrylamide gel, the apparent elastic modulus $G(t=1\text{ s})$ [defined as the inverse of the force-normalized displacement after every 1 s force step, $J(t=1\text{ s})$] is constant, as expected for a linear elastic mate-

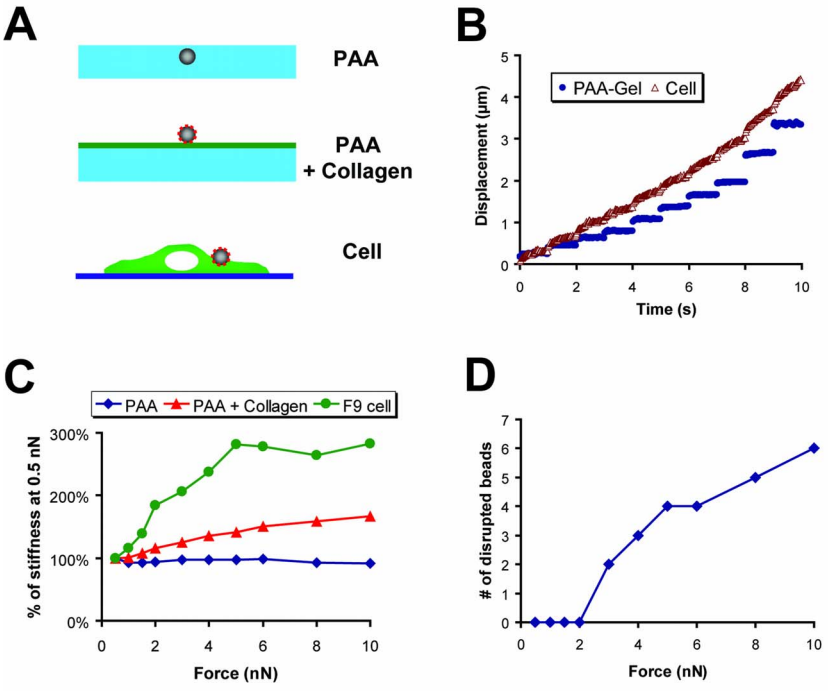


FIG. 5. (Color online) (a) Magnetic beads were embedded into a polyacrylamide (PAA) gel or attached to the surface of a collagen-coated PAA gel, or attached to the apical membrane of cells via fibronectin (FN)-integrin linkages. (b) Displacement of beads embedded into the gel and attached to cells as a response to a stepwise increasing force. Note the purely elastic response of the gel and the viscoelastic creep of the cell. (c) Apparent stiffness $1/J(t=1\text{ s})$ of all three conditions vs applied force. While the gel-embedded beads show linear behaviour, surface-bound beads on PAA gel and cells show different amounts of nonlinearity at higher forces. (d) The amount of disrupted beads vs force is an indicator of bead binding strength.

rial. This serves as a reference and countercheck for the force calibration. Beads coated with fibronectin and attached to polyacrylamide gel with a thin layer of collagen on top show a slightly nonlinear behavior as a result of bead pivoting.[27] Fibronectin-coated beads attached to the surface of adherent cells display a more pronounced nonlinearity and appear increasingly stiffer at higher forces. This nonlinearity can arise both from the properties of the cytoskeleton as well as the geometry of the setting—some beads are completely internalized by the cell while others are loosely bound to the outer membrane and are pulled away from the cell at higher forces. Analyzing the force at which beads detach from the cell surface can also be used to determine membrane binding strength for different ligand coatings [Fig. 5(d)].

Because the forces obtained with this magnetic tweezers design are on the same order of magnitude as the forces generated by cells during adhesion, migration, or cytokinesis,[28] we suggest that the high-force magnetic tweezer setup described here is particularly suitable for studying these biological processes and their underlying regulatory mechanisms.

## ACKNOWLEDGMENTS

We thank Emil Millet (HSPH) for manufacturing the ferrimagnetic beads, Johannes Pauli who developed the initial version of the image acquisition software, Franz Gerst and Dieter Freitag for technical assistance, and Daniel Paranhos Zitterbart for help with the polyacrylamide gels. This work was supported by the Deutsche Forschungsgemeinschaft and the National Institutes of Health, Grant Nos. MA 534/20-4 and HL65960.

[1] A. Heilbronn, Jahrbuch für wiss. Botanik **61**, 284 (1922).
[2] H. Freundlich and W. Seifriz, Z. Phys. Chem., Stoechiom. Verwandtschaftsl. **104**, 233 (1923).
[3] F. H. C. Crick and A. F. W. Hughes, Exp. Cell Res., Suppl. **1**, 37 (1949).
[4] K. Yagi, Comp. Biochem. Physiol. **3**, 73 (1961).
[5] Y. Hiramoto, Exp. Cell Res. **56**, 201 (1969).
[6] F. Amblard, B. Yurke, A. Pargellis, and S. Leibler, Rev. Sci. Instrum. **67**, 818 (1996).
[7] A. H. de Vries, B. E. Krenn, R. van Driel, and J. S. Kanger, Biophys. J. **88**, 2137 (2005).
[8] J. K. Fisher, J. R. Cummings, K. V. Desai, L. Vicci, B. Wilde, K. Keller, C. Weigle, G. Bishop, R. M. Taylor, C. W. Davis, R. C. Boucher, E. T. O'Brien, and R. Superfine, Rev. Sci. Instrum. **76**, 053711 (2005).
[9] J. K. Fisher, J. Cribb, K. V. Desai, L. Vicci, B. Wilde, K. Keller, R. M. Taylor, J. Haase, K. Bloom, E. T. O'Brien, and R. Superfine, Rev. Sci. Instrum. **77**, 023702 (2006).
[10] M. Sato, T. Z. Wong, and R. D. Allen, J. Cell Biol. **97**, 1089 (1983).
[11] W. H. Guilford and R. W. Gore, Am. J. Physiol. **263**, C700 (1992).
[12] F. Ziemann, J. Radler, and E. Sackmann, Biophys. J. **66**, 2210 (1994).
[13] B. G. Hosu, K. Jakab, P. Banki, F. I. Toth, and G. Forgacs, Rev. Sci. Instrum. **74**, 4158 (2003).
[14] M. Barbic, J. J. Mock, A. P. Gray, and S. Schultz, Appl. Phys. Lett. **79**, 1897 (2001).
[15] F. Assi, R. Jenks, J. Yang, C. Love, and M. Prentiss, J. Appl. Phys. **92**, 5584 (2002).
[16] C. Gosse and V. Croquette, Biophys. J. **82**, 3314 (2002).
[17] N. Walter, C. Selhuber, H. Kessler, and J. P. Spatz, Nano Lett. **6**, 398 (2006).
[18] B. D. Matthews, D. R. Overby, F. J. Alenghat, J. Karavitis, Y. Numaguchi, P. G. Allen, and D. E. Ingber, Biochem. Biophys. Res. Commun. **313**, 758 (2004).
[19] A. R. Bausch, F. Ziemann, A. A. Boulbitch, K. Jacobson, and E. Sackmann, Biophys. J. **75**, 2038 (1998).
[20] F. J. Alenghat, B. Fabry, K. Y. Tsai, W. H. Goldmann, and D. E. Ingber, Biochem. Biophys. Res. Commun. **277**, 93 (2000).
[21] H. Huang, J. Sylvan, M. Jonas, R. Barresi, P. T. C. So, K. P. Campbell, and R. T. Lee, Am. J. Physiol.: Cell Physiol. **288**, C72 (2005).
[22] D. R. Overby, B. D. Matthews, E. Alsberg, and D. E. Ingber, Acta Biomaterialia **1**, 295 (2005).
[23] P. A. Valberg and D. F. Albertini, J. Cell Biol. **101**, 130 (1985).
[24] N. Wang, J. P. Butler, and D. E. Ingber, Science **260**, 1124 (1993).
[25] B. Fabry, G. N. Maksym, J. P. Butler, M. Glogauer, D. Navajas, and J. J. Fredberg, Phys. Rev. Lett. **87**, 148102 (2001).
[26] B. Fabry, G. N. Maksym, S. A. Shore, P. E. Moore, R. A. Panettieri, Jr., J. P. Butler, and J. J. Fredberg, J. Appl. Physiol. **91**, 986 (2001).
[27] S. M. Mijailovich, M. Kojic, M. Zivkovic, B. Fabry, and J. J. Fredberg, J. Appl. Physiol. **93**, 1429 (2002).
[28] N. Q. Balaban, U. S. Schwarz, D. Riveline, P. Goichberg, G. Tzur, I. Sabanay, D. Mahalu, S. Safran, A. Bershadsky, L. Addadi, and B. Geiger, Nat. Cell Biol. **3**, 466 (2001).